HHS Public Access

Author manuscript

J Mol Cell Cardiol. Author manuscript; available in PMC 2019 October 01.

Published in final edited form as:

J Mol Cell Cardiol. 2018 October ; 123: 185–197. doi:10.1016/j.yjmcc.2018.09.008.

Phospholamban Regulates Nuclear Ca^{2+} Stores and Inositol 1,4,5-Trisphosphate Mediated Nuclear Ca^{2+} Cycling in Cardiomyocytes

Mu Chen[#1,2], **Dongzhu Xu**[#1,3], **Adonis Z. Wu**[1], **Evangelia Kranias**[4], **Shien-Fong Lin**[1,5], **Peng-Sheng Chen**[1], and **Zhenhui Chen**[1,†]

[1]Krannert Institute of Cardiology, Indiana University, Indianapolis, IN, USA

[2]Department of Cardiology, Xinhua Hospital, School of Medicine, Shanghai Jiao Tong University, Shanghai, China

[3]Cardiovascular Division, Institute of Clinical Medicine, Faculty of Medicine, University of Tsukuba, Japan

[4]Department of Pharmacology and Systems Physiology, University of Cincinnati College of Medicine, Cincinnati, OH, USA

[5]Institute of Biomedical Engineering, College of Electrical and Computer Engineering, National Chiao Tung University, Hsin-Chu, Taiwan

[#] These authors contributed equally to this work.

Abstract

Aims—Phospholamban (PLB) is the key regulator of the cardiac Ca^{2+} pump (SERCA2a)-mediated sarcoplasmic reticulum Ca^{2+} stores. We recently reported that PLB is highly concentrated in the nuclear envelope (NE) from where it can modulate perinuclear Ca^{2+} handling of the cardiomyocytes (CMs). Since inositol 1,4,5-trisphosphate (IP_3) receptor (IP_3R) mediates nuclear Ca^{2+} release, we examined whether the nuclear pool of PLB regulates IP_3-induced nuclear Ca^{2+} handling.

Methods and Results—Fluo-4 based confocal Ca^{2+} imaging was performed to measure Ca^{2+} dynamics across both nucleus and cytosol in saponin-permeabilized CMs isolated from wild-type (WT) or PLB-knockout (PLB-KO) mice. At diastolic intracellular Ca^{2+} ($[Ca^{2+}]_i$= 100 nM), the Fab fragment of the monoclonal PLB antibody (anti-PLB Fab) facilitated the formation and increased the length of spontaneous Ca^{2+} waves (SCWs) originating from the nuclear region in CMs from WT but not from PLB-KO mice. We next examined nuclear Ca^{2+} activities at basal

[†] Address correspondence to: Zhenhui Chen, Ph.D., Krannert Institute of Cardiology and Division of Cardiology, Department of Medicine, Indiana University School of Medicine, 1800 N Capitol Ave, Indianapolis 46202, IN, USA, Tel: 1-317-274-0964, Fax: 1-317-962-0505, zhechen@iu.edu.

Disclosures

None.

condition and after sequential addition of IP_3, anti-PLB Fab, and the IP_3R inhibitor 2-aminoethoxydiphenyl borate (2-APB) at a series of $[Ca^{2+}]_i$. In WT mice, at 10 nM $[Ca^{2+}]_i$ where ryanodine receptor (RyR2) based spontaneous Ca^{2+} sparks rarely occurred, IP_3 increased fluorescence amplitude (F/F_0) of overall nuclear region to 1.19 ± 0.02. Subsequent addition of anti-PLB Fab significantly decreased F/F_0 to 1.09 ± 0.02. At 50 nM $[Ca^{2+}]_i$, anti-PLB Fab not only decreased the overall nuclear F/F_0 previously elevated by IP_3, but also increased the amplitude and duration of spark-like nuclear Ca^{2+} release events. These nuclear Ca^{2+} releases were blocked by 2-APB. At 100 nM $[Ca^{2+}]_i$, IP_3 induced short SCWs originating from nucleus. Anti-PLB Fab transformed those short waves into long SCWs with propagation from the nucleus into the cytosol. In contrast, neither nuclear nor cytosolic Ca^{2+} dynamics was affected by anti-PLB Fab in CMs from PLB-KO mice in all these conditions. Furthermore, in WT CMs pretreated with RyR2 blocker tetracaine, IP_3 and anti-PLB Fab still increased the magnitude of nuclear Ca^{2+} release but failed to regenerate SCWs. Finally, anti-PLB Fab increased low Ca^{2+} affinity mag-fluo 4 fluorescence intensity in the lumen of NE of nuclei isolated from WT but not in PLB-KO mice.

Conclusion—PLB regulates nuclear Ca^{2+} handling. By increasing Ca^{2+} uptake into lumen of the NE and perhaps other perinuclear membranes, the acute reversal of PLB inhibition decreases global Ca^{2+} concentration at rest in the nucleoplasm, and increases Ca^{2+} release into the nucleus, through mechanisms involving IP_3R and RyR2 in the vicinity.

Keywords

Phospholamban; calcium signaling; cardiomyocyte; nuclear membranes; 1,4,5-trisphosphate receptor; sarcoplasmic reticulum Ca^{2+} cycling; nuclear Ca^{2+} dynamics

1. Introduction

Phospholamban (PLB) regulates cardiac sarcoplasmic reticulum (SR) Ca^{2+}-ATPase (SERCA2a isoform), controlling the rate of Ca^{2+} removal from the cytoplasm into the lumen of SR [1–3]. In cardiomyocytes (CMs), phosphorylation of PLB or the use of anti-PLB antibody reverses its inhibition on SERCA2a, thus enhancing the Ca^{2+} uptake into SR and the subsequent SR Ca^{2+} release through ryanodine receptor (RyR2) which triggers excitation-contraction (E-C) coupling [1, 2, 4]. The critical role of PLB in regulation of cardiac contractility has been demonstrated in multiple experimental systems: *in vitro* expression systems, PLB knockout (PLB-KO) and transgenic mice [5, 6], and by the effects of that naturally occurring mutations of PLB [7–9] that cause human heart diseases. Therefore, PLB remains as an important target for understanding cardiac function in physiological and pathological conditions and for new drug design aiming at the control of intracellular Ca^{2+} handling.

Nuclear Ca^{2+} signaling exists in CMs as well as other types of cells, and critically regulates various essential cell functions [10, 11]. In CMs, Bers and colleagues proposed an “excitation-transcription coupling” mechanism that links the local nuclear Ca^{2+} release through 1,4,5-trisphosphate (IP_3) receptor (IP_3R) to gene regulation [12], which is separated from the global SR mediated E-C coupling. While cytosolic Ca^{2+} release is dominated by RyR2 release from SR, IP_3R mediated Ca^{2+} signaling is prominently responsible for nuclear Ca^{2+} handling in ventricular CMs [12]. Several groups showed that IP_3 induced the opening

of IP_3R channels in the nuclear envelope (NE), decreased Ca^{2+} content in the nuclear Ca^{2+} stores (inside the lumen of perinuclear endoplasmic reticulum and NE), and subsequently increased Ca^{2+} concentration inside the nucleus [12, 13] [14], and global Ca^{2+} release, e.g., from both SR and NE [15]. Luo *et al* showed that such nuclear Ca^{2+} release may be in the form of nuclear sparks and waves in neonatal rat CMs [16]. In addition to IP_3R, RyR-based Ca^{2+} release in the nuclear regions may also co-exist [17, 18], but details remain unclear [13, 19–24]. In parallel to SR Ca^{2+} uptake, SERCA2a is responsible for recycling Ca^{2+} into lumen of NE, yet detailed mechanisms for the regulation of nuclear Ca^{2+} handling remain poorly understood.

We recently showed that PLB protein exists outside of the conventional sarcomeric SR network, where it resides within the NE of CMs [25]. The high concentration of PLB in the NE is confirmed in both CMs and in isolated cardiac nuclei from several species, including humans, by multiple species-specific monoclonal anti-PLB antibodies [25]. In contrast, SERCA2a distributes evenly between NE and SR. Administration of isoproterenol, which phosphorylates PLB, increased the fluorescence amplitude and shortened the decay time of Ca^{2+} transients at both cytosolic and nuclear regions, suggesting that detailed Ca^{2+} dynamics may affect SR and perinuclear regions differently.

We have previously characterized a novel reagent, anti-PLB Fab (the Fab fragment of the anti-PLB monoclonal antibody 2D12), which specifically binds to PLB *in situ* in permeabilized CMs [26]. Furthermore, anti-PLB Fab reverses the inhibition of PLB on SERCA2a activity, and facilitates the generation of whole cell propagating spontaneous Ca^{2+} waves (SCWs) traversing through both cytosol [26] and nucleus [25]. The changes in parameters in the perinuclear Ca^{2+} uptake and release in these experiments are consistent with previously documented biophysical characteristics of perinuclear Ca^{2+} release from several other labs [12, 16, 18, 24, 27]. Based on these findings, we hypothesized that PLB in the NE may regulate SERCA-based Ca^{2+} uptake into the nuclear Ca^{2+} stores, influencing perinuclear/nuclear Ca^{2+} dynamics, an important process for transcriptional control. In the current study, taking advantage of anti-PLB Fab and well-characterized PLB-KO mice as a control, we performed detailed analyses of the effects of PLB on Ca^{2+} uptake into the lumen of the NE and subsequent perinuclear Ca^{2+} releases through both IP_3R and RyR2.

2. Methods

2.1 Cardiomyocyte preparation and permeabilization and cardiac nuclei isolation.

The use of animals in the study was approved by the IACUC of Indiana University School of Medicine and the Methodist Research Institute, Indianapolis, Indiana and conformed to the NIH Guide for the care and use of laboratory animals. CM isolation from adult C57BL/6 mice and PLB-KO mice (2 to 6 month old) using protocols modified from our previously reported [26, 28]. In brief, CMs were isolated with 15μg/ml liberase (Roche) stored in normal Tyrode's solution containing (in mM/L): 138 NaCl, 5.33 KCl, 0.33 NaH_2PO_4, 1.18 $MgCl_2$, 10 HEPES, 10 taurine, and 10 glucose, pH 7.4 (NaOH). Small chunks of dog heart tissues were digested with gentle shaking at 37°C for 30 min. Isolated dog CMs were harvested by centrifugation. Permeabilization with saponin (50μg/ml) was conducted for 60

s in a mock internal solution composed of (in mM/L) 100 potassium aspartate, 20 KCl, 10 HEPES, 0.5 EGTA, and 0.75 $MgCl_2$, pH 7.2 (KOH).

Crude cardiac nuclei were isolated based on our modified protocols previously reported [25]. Briefly, mouse CMs were homogenized in low salt solution and centrifuged at 500Xg. Pellets were resuspended in 250mM sucrose, 20mM KCl, 1mM MgCl2, 50mM Tris, (pH 7.0). Crude nuclei were harvested by centrifugation at 1000Xg.

2.2 Confocal immunofluorescence microscopy.

Confocal immunofluorescence microscopy on paraformaldehyde fixed isolated mouse CMs was performed as previously described [26]. The monoclonal antibodies against PLB (2D12) was visualized using Protein A labeled with Alexa-Fluor 594 fluorescent dye. Anti-PLB Fab was conjugated with Alexa-Fluor 594 (ThermoFisher Scientific) in the assay [26].

2.3 Intracellular/nuclear Ca^{2+} imaging and analysis.

Intracellular Ca^{2+} activities were imaged at room temperature with the Leica TCS SP8 LSCM inverted microscope fitted with a 40× 1.42 NA oil immersion objective. Intact CMs were loaded with Fluo-4AM and imaged in normal Tyrode's solution with 1.8 mM Ca^{2+}. Spontaneous Ca^{2+} activity of saponin-permeabilized CMs was imaged using the Ca^{2+} indicator dye Fluo-4, as previous described [26]. The Scan-line was placed across the length of the cell in a medial plane that showed the full nuclear diameter with brighter fluo-4 signal. The z section thickness is 580nm under our experimental setting. Mock internal solution contained (in mM): 100 potassium aspartate, 20 KCl, 5 KH_2PO_4, 5 MgATP, 10 phosphocreatine, 5 U/ml creatine phosphokinase, 10 HEPES, 0.5 EGTA, 1 $MgCl_2$, 0.015 Fluo-4 (Invitrogen), and 8% w/v dextran (molecular weight 40,000), pH 7.2 (KOH). Since fluo-4 was not calibrated, paired experiments were performed to compare the effect of anti-PLB Fab. Use of IP_3 and 2-APB followed protocols of Zima et al [13]. In some experiments, lumenal Ca^{2+} was visualized with use of a low affinity Ca^{2+} indicator Mag-Fluo-4 (ThermoFisher Scientific). In brief, because of the poor signal to noise ratio in mouse CMs, permeabilized dog CMs, or crude mouse cardiac nuclei were incubated with mag-fluo-4 for 30 min in mock internal solution with 50 nM Ca^{2+}, and imaged. $CaCl_2$ was added to make the free $[Ca^{2+}]_i$ of 10nM, 50nM, and 100nM (WebMaxC Extended (http://www.maxchelator.stanford.edu)).

2.4 Statistical analysis.

Results were expressed as mean ± SEM. The statistical significance was evaluated using paired or unpaired *t* tests and one-way ANOVA followed by Tukey post hoc analyses. A value of $p<0.05$ was considered a statistically significant difference.

3. Results

3.1 Effect of anti-PLB on cytosolic and perinuclear originated spontaneous Ca^{2+} waves.

We previously reported that acute reversal of PLB inhibition by anti-PLB Fab significantly increased cytosolic Ca^{2+} release, facilitating the propagation of SCWs in CMs isolated from WT mice [26]. Although anti-PLB Fab acts specifically on PLB, the specificity of the

reagent was not tested in CMs from PLB-KO. In addition, detailed study was not performed to evaluate the effect of anti-PLB Fab on nuclear Ca^{2+} activity at various $[Ca^{2+}]_i$. Here, using saponin-permeabilized CMs isolated from WT and PLB-KO mice, we extended the study to measure the effect of anti-PLB Fab on intracellular Ca^{2+} activity across the cytosol and nucleus.

At 50 nM of $[Ca^{2+}]_i$, line-scan confocal Ca^{2+} images revealed Ca^{2+} sparks and macro sparks in the cytosol (Fig. 1Aa, *Ctl*). Addition of anti-PLB Fab (100 μg/mL) significantly increased Ca^{2+} releases, in the forms of macro-sparks and mini waves in the cytoplasm, consistent with our recent report [26]. Anti-PLB Fab also significantly increased Ca^{2+} releases across the nuclear region (Fig. 1Aa, *Fab*, between *red line*). Fig. 1Ab and c show the intensity profile of the Ca^{2+} release in cytosol and across the nuclear regions, and corresponding fold of increase in spark frequency after addition of anti-PLB Fab. Anti-PLB Fab induced a significantly stronger response of increase in frequency of Ca^{2+} sparks in nucleus than cytosol. In support of PLB action in the NE, addition of anti-PLB Fab failed to stimulate significant subcellular Ca^{2+} release at both cytosolic and nuclear regions in CMs isolated from PLB-KO mice (Fig. 1B). Note that the frequency and intensity of sparks and macro-sparks were higher in PLB-KO than that in WT mice, confirming reports on sarcomeric PLB from multiple labs [29]. Finally, both 2D12 and anti-PLB Fab stained CMs from WT mice, with typical higher immunofluorescence intensity in and around the nucleus than that in SR. However, neither 2D12 nor anti-PLB Fab stained CMs from PLB-KO mice (Fig. 1C), demonstrating the specificity of the anti-PLB Fab in binding to PLB and reversing PLB inhibition of SERCA2a.

As expected, 100 nM $[Ca^{2+}]_i$ increased the frequency of Ca^{2+} sparks and short SCWs under basal conditions in CMs from WT mice (Fig. 2Aa, *Ctl*). Compared with those in the cytosol, the spontaneous Ca^{2+} waves (SCWs) across nuclei exhibited the characteristics of perinuclear Ca^{2+} transients [18, 24, 25, 27, 30], with smaller amplitude (F/F_0) and slower rise and decay time (Fig. 2Ab, compare black vs blue traces). Consistent with our previously report [26], addition of anti-PLB Fab significantly increased initiation of short and long SCW in the cytosol (Supplement Figure 1). Interestingly, addition of anti-PLB Fab also significantly increased long SCWs that were initiated in the perinuclear region and propagated into the cytosol (Fig.2Aa, *Fab,* between red lines, magnified in panel Ab). Fig. 2Ac summarizes our findings. In addition to the significant increase in amplitude (F/F_0), anti-PLB Fab also decreased the half decay time (DT_{50}) , reflecting the reversal of PLB inhibition of SERCA2a, causing a higher rate of Ca^{2+} re-uptake into SR and NE. Due to low density of RyRs and low effective Ca^{2+} diffusion coefficients in the nucleus [31], the wave velocity in the perinuclear region was slower than that in the cytosol, but both were increased after addition of anti-PLB Fab. On the other hand, CMs isolated from PLB-KO already have greater levels of intracellular Ca^{2+} release than that in WT, leading to a high frequency of short broken SCWs at both cytosolic [32] and nuclear regions (Fig. 2Ba). Subsequent addition of anti-PLB Fab had no effect on SCWs in both cytosol and nuclear regions in CMs from PLB KO mice (Fig. 2Ba, amplified in panel Bb, kinetic parameters summarized in panel Bc).

Fig. 2C and D compared the differences before and after addition of anti-PLB Fab on frequencies of mini and long SCWs between WT and PLB-KO. While very few long SCWs were developed at basal condition in WT mice, 35.4 ± 5.1% of short SCWs were originated within the nuclear regions. Anti-PLB Fab application dramatically increased the total frequency of long SCWs (from 0.05 ± 0.03 to 0.52 ± 0.07 Hz) and long SCWs which initiated from nuclear region and propagated into the cytosol (from 0.02 ± 0.02 to 0.24 ± 0.05 Hz). Note that 43.3 ± 7.6% of long SCWs were initiated in the nuclear regions. In contrast, anti-PLB Fab did not change the frequencies or morphologies of SCWs in PLB-KO. As nuclei only occupied 18 ± 1% of the whole line-scan regions, we compared SCWs density originated from cytosol or nucleus region by dividing the frequency of SCWs initiated in either region by the width of corresponding region. In WT, SCW density exhibited no significant difference between cytosol and nucleus at basal condition. However, anti-PLB Fab caused about 8 fold increase in the SCW density in cytosol (1000 × Hz/μm: 0.4 ± 0.3 vs. 3.4 ± 0.5, $p<0.05$), compared to a more than 12 fold increase in the nuclear region (1000 × Hz/μm: from 1.1 ± 1.1 to 14.6 ± 2.9, $p<0.05$). In contrast, these effects were not observed in PLB KO mice. Collectively, these sets of data suggest that acute reversal of PLB inhibition by anti-PLB Fab enhances the SERCA-based Ca^{2+} uptake into SR and more profoundly into the nuclear Ca^{2+} stores, and increases the frequencies of whole cell propagating long SCWs, especially SCWs originated from nuclear regions.

3.2 Effect of ET-1 on Ca^{2+} transients in intact cardiomyocytes isolated from WT and PLB-KO

Since nuclear Ca^{2+} release involves IP_3R [12, 16, 24], we used endothelin-1 (ET-1, 100 nM) to activate IP_3R and measured Ca^{2+} transients in intact CMs isolated from WT and PLB-KO mice. As shown in Fig. 3A, ET-1 increased Ca^{2+} releases in the cytosol but more prominently across the nuclear region, consistent with reports from other labs using ventricular CMs from rat [14, 27] and rabbit [15]. In particular, ET-1 significantly increased diastolic F/F_0 at rest to 1.18 ± 0.03 and systolic Ca^{2+} transients F/F_0 from 5.5 ± 0.2 to 8.6 ± 0.2 in the nuclear regions. Interestingly, ET-1 decreased nuclear Ca^{2+} transients DT_{50} from 367.6 ± 14.0 ms to 279.9 ± 13.4 ms in WT. However, while F/F_0 of Ca^{2+} transients increased, DT_{50} was not altered by ET-1 (from 158.3 ± 6.6ms to 174.1± 22.5 ms, $p>0.05$) in PLB-KO. Those different effects of ET-1 on perinuclear Ca^{2+} handling between WT and PLB-KO indicate that PLB may be involved in regulation of IP_3R-mediated perinuclear Ca^{2+} handling.

3.3 Effect of anti-PLB Fab on nuclear Ca^{2+} levels of cardiomyocytes in the presence of IP_3.

Because ET-1 has broad effects in intact CMs, we used anti-PLB Fab to manipulate PLB specifically and determine whether PLB contributes to the modulation of IP_3-induced nuclear Ca^{2+} handling at a series of $[Ca^{2+}]_i$. We first examined 2D Ca^{2+} imaging at 10 nM of $[Ca^{2+}]_i$ where RyR2 based spontaneous Ca^{2+} release rarely occurs. Addition of IP_3 (10 μM) increased fluo-4 fluorescence (F/F_0) at rest in cytosol (*Cy*) and more prominently in nucleus (*Nu*) in permeabilized CMs from both WT (Fig. 4A and 4B) and PLB-KO (Fig. 4C and 4D). In particular, F/F_0 at rest across the nucleus increased to 1.19 ± 0.02 and 1.17 ± 0.02 for CMs from WT and PLB-KO, respectively, a level similar to that previously

reported in atria CMs [13], suggesting increased nuclear Ca^{2+} releases through opening of IP_3R channels. IP_3 also had some effects on F/F_0 at rest in the cytoplasmic region, to 1.08 ± 0.02 and 1.08 ± 0.02 for WT and PLB-KO, respectively. Importantly, subsequent addition of anti-PLB Fab significantly decreased F/F_0 at rest in cytosolic regions to 1.04 ± 0.02 and more profoundly in the nuclear regions to 1.09 ± 0.02 in CMs from WT mice. In contrast, anti-PLB Fab had no effect on F/F_0 at rest in CMs from PLB-KO mice in nuclear (1.17 ± 0.03) and cytosolic regions (1.07 ± 0.02). Further addition of IP_3R blocker 2-aminoethoxydiphenyl borate (2-APB, 10 μM) decreased F/F_0 at rest in both regions of CMs from WT (Nu: 1.03 ± 0.02 and Cy: 1.01 ± 0.02) and PLB-KO mice (Nu: 1.05 ± 0.02 and Cy: 1.00 ± 0.02). These results were also verified by line-scan images at 10 nM of $[Ca^{2+}]_i$ (Supplement Fig.2). Therefore, acute reversal of PLB inhibition by anti-PLB Fab increases SERCA uptake, thus responsible for the transient reduction in nuclear Ca^{2+} until a new IP_3R release-uptake balance is reached.

We next performed the experiments using 50 nM of $[Ca^{2+}]_I$ to induce spontaneous Ca^{2+} sparks. As shown in Fig. 5, effects of IP_3 and anti-PLB Fab on F/F_0 at rest in nuclear regions were similar to that observed in 10 nM $[Ca^{2+}]_i$, but more complicated for nuclear Ca^{2+} releases. Specifically, while having small effects in the cytoplasmic region (Fig. 5. *Cy,* bottom panels, 1.04 ± 0.02 and 1.04 ± 0.02 at 4min, for WT and PLB-KO, respectively), IP_3 significantly increased F/F_0 at rest across nuclear regions with time (top panels, *Nu*) to 1.14 ± 0.03 and 1.13 ± 0.02 at 4 min for CMs from WT (Fig. 5A,B) and PLB-KO (C,D), respectively. Again, subsequent addition of anti-PLB Fab significantly decreased F/F_0 at rest in the nuclear regions to 1.06 ± 0.02 at 3min only in CMs isolated from WT (A,B) but not from PLB-KO (C,D. at 3min,1.12 ± 0.02). Consistent with our previous report [26], anti-PLB Fab also decreased F/F_0 at rest in the cytosol (0.98 ± 0.02) in CMs from WT, but had no effect on CMs from PLB-KO mice. In addition, IP_3R blockade by 2-APB further decreased F/F_0 at rest to 1.01 ± 0.02 in nuclear regions of CMs from both WT and PLB-KO. These results confirmed the observations at 10nM $[Ca^{2+}]_i$, suggesting reversal of PLB inhibition by anti-PLB Fab reduces nuclear Ca^{2+} concentrations elevated by IP_3-induced perinuclear/nuclear Ca^{2+} release.

Interestingly, at 50 nM of $[Ca^{2+}]_i$, while IP_3 showed no significant effect on Ca^{2+} sparks in the cytosol, nuclear Ca^{2+} release showed significant increases in the frequency of “nuclear spark-like” Ca^{2+} releases in the nuclear regions of both CMs from WT (Fig. 5A) and PLB-KO (Fig. 5C). Kinetic parameters of those sparks are listed in Table 1. In general, Ca^{2+} releases in the nuclear regions were significantly different in morphology from that of the cytosol (compare top and bottom traces). Compared with sparks in the cytosol, nuclear Ca^{2+} sparks have smaller F/F_0 and full width at half maximum (FWHM), but larger full duration at half maximum (FDHM) and DT_{50} (Table 1), consistent with characteristics of “nuclear sparks” reported previously [16]. Importantly, anti-PLB Fab generated even bigger, prolonged Ca^{2+} releases in the nuclear regions in CMs from WT, but not PLB-KO (compare *arrows in Nu*). Table 1 shows that in WT CMs, anti-PLB Fab significantly increased F/F_0, FWHM and FDHM, but decreased DT_{50} in the nuclear regions. In contrast, at basal condition, CMs from PLB-KO exhibited more frequent, bigger and prolonged IP_3-induced Ca^{2+} releases in the nuclear regions than those in WT. Anti-PLB Fab had no additional effect on either cytosolic or nuclear regions, confirming that the observed effects in WT

were attributed to the reversal of PLB inhibition by anti-PLB Fab. These results demonstrate that PLB in the NE regulates IP_3R-mediated perinuclear/nuclear Ca^{2+} release.

As $[Ca^{2+}]_i$ further increased to 100 nM, macro sparks and short SCWs occurred at basal conditions in WT. The addition of IP_3 induced more organized short SCWs originating in and confining within the nucleus (Fig. 6A). Subsequent addition of anti-PLB Fab significantly increased F/F_0 and decreased DT_{50} of SCWs (Fig. 6C). Importantly, anti-PLB Fab transformed the nucleus-originating short waves into long SCWs that propagated outside the nucleus, triggering subsequent cytosolic Ca^{2+} release (Fig. 6A). In contrast, in PLB-KO (Fig. 6B), IP_3 alone increased the frequency of short and long SCWs originating in the nucleus which spread into cytosol. Subsequent addition of anti-PLB Fab affected neither the frequency nor other biophysical parameters of the SCWs (Fig. 6C).

3.4 Effects of anti-PLB Fab with inhibition of RyR by tetracaine

To separate the effects of RyR2 from IP_3R on Ca^{2+} release in the nuclear regions, at 100 nM $[Ca^{2+}]_i$, we pretreated WT CMs with RyR blocker tetracaine (0.5mM), followed by addition of IP_3, anti-PLB Fab, and 2-APB. As shown in Fig. 7, tetracaine blockade of RyR2 was evident as SCWs were completely eliminated. Subsequent application of IP_3 increased F/F_0 at rest intensity and augmented Ca^{2+} release in the nuclear regions, consistent with previous observation in atrial and neonatal ventricular myocytes [16, 20]. Anti-PLB Fab decreased F/F_0 at rest and further increased Ca^{2+} release in the nuclear regions (F/F_0 from 1.8 ± 0.1 to 2.1 ± 0.1, $p<0.05$). However, no SCW was formed with RyR blockade even in the presence of IP_3 and anti-PLB Fab. Finally, IP_3R blockade by 2-APB eliminated all Ca^{2+} release in the nuclear regions. These results suggest that PLB modulates IP_3R-mediated Ca^{2+} release in the nuclear regions, but RyR activities are necessary to form propagating SCWs originating from nuclear regions.

3.5 Effects of anti-PLB Fab on lumenal Ca^{2+} in the NE and SR.

To directly address whether PLB regulates Ca^{2+} uptake into the lumen of the NE, we measured the effect of anti-PLB Fab on lumenal Ca^{2+} inside the NE and SR. Thus, the lumen of permeabilized dog CMs was loaded with mag-fluo-4 and imaged at 50 nM Ca^{2+}. In control experiment in the absence of IP_3, there was no significant change in mag-fluo-4 fluorescence intensity inside the NE and SR for 30 min (Fig. 8Aa). We then confirmed the results previously reported by Wu and Bers [33] that addition of IP_3 caused Ca^{2+} releases from lumen. Indeed, IP_3 significantly decreased the mag-fluo-4 intensity (Fig. 8Ab) to about 42.1 ± 1.6 % for SR and 49.2 ± 1.5 % for NE at 20 min after its application, reaching a new balance between Ca^{2+} uptake and release. Addition of anti-PLB Fab significantly increased fluorescence intensity to about 116.4 ± 0.8% for the NE and 110.9 ± 0.9% for SR (Fig. 8Ac), indicating that reversal of PLB inhibition of SERCA increased Ca^{2+} concentration inside the lumen of NE and SR. Importantly, when anti-PLB Fab was present, addition of IP_3 decreased the levels fluorescence intensity to about 76.4 ± 1.4% in the NE and 73.4 ± 1.7% in SR, compared to the absence of anti-PLB Fab. These findings indicate that a new balance was reached at higher lumenal Ca^{2+} concentration, due to increased SERCA uptake. Furthermore, anti-PLB Fab prolonged the decay time for IP_3 induced fluorescence decay (Fig. 8Ad). The difference in these parameters between NE and SR was small, consistent

with the previous finding by Wu and Bers [33] that the lumen of NE and SR are contiguous to maintain overall uniform driving force.

Because the lumen of SR and NE are contiguous, we measured specifically if anti-PLB Fab increases NE lumenal Ca^{2+} in isolated mouse cardiac nuclei. As shown in a typical experiment, anti-PLB Fab significantly increased mag-fluo 4 fluorescence intensity around the nucleus from WT mice (to 110.7 ± 2.0 %, Fig. 8B). In contrast, no significant change was observed on the mag-fluo-4 fluorescence intensity in isolated cardiac nuclei from PLB-KO after addition of anti-PLB Fab (to 99.8 ± 1.0 %, Fig. 8B). These results demonstrate for the first time that PLB regulates Ca^{2+} uptake into the lumen of the NE and IP_3-induced Ca^{2+} release.

4. Discussion

In this study, we further investigated our recent findings that relatively high concentrations of PLB exist in the nuclear region, likely to be in the NE, of CMs. Moreover, we have shown that PLB in the nuclear region regulates SERCA-mediated Ca^{2+} uptake into perinuclear/nuclear lumens, and that its subsequent release may involve both IP_3R and RyR in the vicinity.

4.1 PLB and the Ca^{2+} waves originated in the nucleus in CMs.

Several previous studies reported that Ca^{2+} sparks and waves may originate in nuclei of atrial myocytes [13, 34], in neonatal rat CMs [16], and in adult mouse ventricular CMs [18]. While some of those waves were confined inside nucleus, nuclear Ca^{2+} waves can also spread into the cytosol, capable of inducing whole cell propagating Ca^{2+} waves [16]. In particular, retention of CSQ2 (CSQ2-DsRed) in the NE can increase SCWs initiated in the perinuclear/nuclear regions in CMs isolated from both WT and IP_3R2 knockout mice [18]. While opening of RyR or IP_3R may be responsible for these nuclear Ca^{2+} release, it is unclear whether PLB is involved in the regulation of these Ca^{2+} waves originated in the nucleus. Here under basal condition in the semi-intact CMs, we showed that SCWs exhibit similar probabilities of initiation from cytosol and nucleus when normalized to the width of the line-scan region. Anti-PLB Fab-increased SR Ca^{2+} content may trigger a RyR lumenal Ca^{2+} sensor [35], increasing the channel open probability. On the other hand, the volume of nuclear Ca^{2+} stores are likely several orders of magnitude smaller than that of SR, given the large surface area of SR membranes. Using our anti-PLB antibody to reverse total SERCA inhibition in all PLB-containing compartments, we revealed how transient increases in Ca^{2+} concentration occur differently in perinuclear regions and SR. Although Fluo-4 based Ca^{2+} wave measurement has the limitation and cannot pinpoint the origin of the Ca^{2+} release, we speculate that anti-PLB Fab may induce a much stronger response in the perinuclear regions than in the cytosol, prominently increasing incidents of SCWs that originate in the nucleus, and unmasking PLB-dependent initiation of SCWs in nuclear regions.

In intact CMs, complex regulatory pathways, e.g., adrenergic stimulation, could regulate phosphorylation and dephosphorylation differently in nuclear regions and SR, resulting in differential Ca^{2+} load in nuclear regions and SR. Furthermore, there are differences in the proximity of the Ca^{2+} uptake and releasing units, as well as their properties (e.g., density,

sensitivity) in these sub-compartments for achieving various physiological functions. Therefore, SCWs initiating in the nuclear regions may not contribute equally or proportionally to the overall intracellular Ca^{2+} dynamics under basal and physiological conditions. However, during pathological conditions, cardiac remodeling during hypertrophy and heart failure has been shown to change SR and nuclear Ca^{2+} dynamics, along with increased size of the nuclei [24]. For example, in an early hypertrophy rat model, nuclear Ca^{2+} signaling was enhanced with elevated nuclear SERCA2a expression relative to the cytoplasm, [36]. However, nuclear PLB dysfunction was not studied in these disease conditions. Higher sympathetic tone during heart failure might also selectively phosphorylate PLB in the NE, leading to the effects similar with those shown in this study. Combinations of these factors could increase the incidence of long SCWs originating in the nucleus, potentially changing the normal balanced action from cytoplasmic and nuclear regions into imbalanced overall abnormal Ca^{2+} dynamics, and enhanced vulnerability to arrhythmias during heart failure.

Various mutations of PLB have been linked to lethal cardiomyopathies in human patients. In particular, patients harboring PLB mutation R25C-PLB or R14Del-PLB developed hypertrophy and arrhythmia [9, 37]. Both PLB mutants were shown to exhibit abnormal Ca^{2+} dynamics in CMs, with as-yet unknown molecular and cellular mechanisms [38]. Interestingly, R14Del-PLB exhibited abnormal perinuclear accumulations and was mis-routed during trafficking that resulted in its absence from SR [39]. The extent of SCWs originating in the nucleus, however, was not further studied in these PLB mutants (or any other PLB mutants). Coordinated studies with regard to PLB regulation are necessary to understand the full impact of PLB and PLB mutants on both SR and nuclear Ca^{2+} cycling in physiological and pathological conditions in intact CMs.

4.2 Different Ca^{2+} dynamics in CMs from PLB-KO and WT mice treated with anti-PLB Fab

Our study used the important research tools of anti-PLB Fab and the well-characterized PLB-KO mice. In fact, the use of PLB-KO model as a control validated the specificity of binding interaction of anti-PLB Fab to PLB. Anti-PLB Fab, along with an array of monoclonal anti-PLB antibodies, neither stained nor affected SR and nuclear Ca^{2+} dynamics in CMs isolated form PLB-KO mice. Therefore, considering that various reagents, including beta-adrenergic stimulation, which have several possible protein targets in addition to PLB, anti-PLB Fab remains as a specific tool to probe PLB and other factors in intracellular Ca^{2+} handling [25].

Studies combining the use of anti-PLB Fab on WT mice with PLB-KO controls clearly demonstrated the contribution of PLB to the initiation and maintenance of SCWs in SR and nuclear regions. In WT mice, anti-PLB Fab reduced the decay time DT_{50} of SCWs, a hallmark effect of PLB. Reduced DT_{50} of SCWs was also observed at basal condition in CMs from PLB-KO mice. However, there are marked differences in Ca^{2+} dynamics between PLB-KO and WT CMs in the absence and presence of anti-PLB Fab. In line with other published findings [29], we observed that CMs in PLB-KO displayed higher frequency of Ca^{2+} sparks than those in WT. In addition, while SCWs in PLB-KO typically appeared with short broken wave forms [32, 40], SCWs in WT exhibited whole cell propagating SCWs in

the presence of anti-PLB Fab. This anti-PLB Fab effect can be explained by the wave sensitization model [41], in which acute PLB ablation in CMs from WT mice increased Ca^{2+} uptake into SR, promoting the formation and elongation of SCWs.

Chronic absence of PLB in PLB-KO mice has been reported to exhibit adaptive changes in intracellular Ca^{2+} handling proteins [42]. In particular, RyR2 expression in PLB-KO mice is decreased more than 25%, which could contribute to the occurrence of short travelling of SCWs. Additionally, it is well established that a hyperdynamic cardiac function of PLB-KO mouse is associated with increases in inotropy but not chronotropy [5]. While human PLB null resulted in lethal cardiomyopathy [8], neither arrhythmias nor other cardiac phenotypes were observed in PLB-KO mice, which was possibly attributed to these adaptations. Nevertheless, in the current study, we did observe differences in nuclear Ca^{2+} handling in CMs from PLB-KO mice, including different responses to ET-1 and IP_3 treatments (table 1) and more frequent nucleus-initiated SCWs in PLB-KO than WT at basal condition (Fig.2). Coupled with our findings using anti-PLB Fab in WT CMs, because of the importance of PLB to nuclear Ca^{2+} handling, it is also possible that adaptation in nuclear Ca^{2+} handling proteins may also occur in PLB-KO mice. Although previous 2D gel based proteomic studies did not identify IP_3R alteration in PLB-KO [43], further detailed studies will be necessary to address such potential changes. In addition, future studies on this valuable line of mice will be helpful to dissect the mechanism of nuclear Ca^{2+} handling in CMs.

4.3 Profound effects of PLB on nuclear Ca^{2+} signaling

Anti-PLB Fab significantly increased Ca^{2+} uptake into the lumenal nuclear Ca^{2+} stores and decreased overall IP_3-induced levels of nucleoplasmic Ca^{2+} only in CMs from WT, not CMs from PLB-KO. A likely mechanism for this effect would appear to be that SERCA uptake into perinuclear and nuclear Ca^{2+} stores was enhanced by acute reversal of PLB inhibition. Previously, Ljubojevic *et al* detected the presence of significant nucleoplasmic-to-cytoplasmic $[Ca^{2+}]$ gradients in resting myocytes and during the cardiac cycle [44]. They suggested that regulation of the nucleoplasmic $[Ca^{2+}]$ in CMs may be through diffusion from the cytoplasm and Ca^{2+}release via IP_3R from perinuclear Ca^{2+} stores. Our data here strongly suggest that PLB must also be involved in this mechanism to regulate nucleoplasmic $[Ca^{2+}]$ in CMs. In parallel, in the presence of IP_3, reversal of PLB inhibition also increased intra-nuclear Ca^{2+} release, in the form of discrete macro sparks and SCWs that originated in the nuclear regions. Increased driving force is a likely mechanism due to the augmentation of $[Ca^{2+}]$ inside the NE by anti-PLB Fab. However, the mechanism behind the nuclear Ca^{2+} release events is complex and less clear.

Ca^{2+} release through IP_3R channels (puff) are normally very small in amplitude. At our experimental conditions, we do not think we directly recorded individual puffs. For example, at 10nM $[Ca^{2+}]_i$, no individual releasing events was recorded, although IP_3 induced a significant rise in F/F_0. At 50nM $[Ca^{2+}]_i$, IP_3 significantly increased frequency of macro spark-like nuclear Ca^{2+} releases, but no other parameters were significantly affected in WT (Table 1). Nonetheless, IP_3R is likely to be involved in these spark-like nuclear Ca^{2+} release events because of their activation by IP_3 and inhibition by 2-APB. A small event in the cytosol/perinuclear region can become greater in magnitude in the nucleus due to its lower

buffering than in the cytosol [45]. Therefore, it is possible that those spark-like local nuclear Ca^{2+} release are combined effects of IP_3R (puffs) and RyR (sparks). For example, nuclear Ca^{2+} release through IP_3R increase local Ca^{2+} concentration, synergistically increasing perinuclear/nuclear RyR2 open probability.

The nature of SCWs originating in cardiac nuclei has remained uncertain, although it is suggested that IP_3R and RyR2 could both be involved [14–16, 18]. Gating of IP_3R involves a multitude of factors, including ligands, cytoplasmic and luminal Ca^{2+} sensors and channel cooperativity [46]. At 100nM $[Ca^{2+}]_i$ with tetracaine and IP_3 pretreatment, reversal of PLB inhibition increased the amount of Ca^{2+} release (F/F_0), but failed to regenerate SCWs (Fig. 7). Hence, even with weakened RyR Ca^{2+} release, Ca^{2+} release through IP_3R is not sufficient to form SCWs. Interestingly, in spontaneously hypertensive rats, increased IP_3R Ca^{2+} release has been shown to augment Ca^{2+} transients [27]. In conclusion, acute reversal of PLB inhibition raises perinuclear Ca^{2+} content, leading to increased nuclear Ca^{2+} release via activation of IP_3R, which may trigger perinuclear/nuclear RyR in a positive feedback mechanism to generate SCWs from the nucleus.

4.4 Specific PLB regulation of the lumenal Ca^{2+} concentration in the NE and SR.

There is a PLB concentration gradient between the NE and SR [25]. Therefore, under certain conditions, the rate of SERCA Ca^{2+} uptake can be distinct for perinuclear and nuclear membranes and SR, creating different Ca^{2+} concentration locally in the lumen of NE and SR. If SR and NE membranes are actually connected, an overall uniform driving force for Ca^{2+} release will be maintained [33]. As a result, differences between Ca^{2+} concentration in the lumen of NE and SR would only be local and transient, and not detectable in our current experimental approaches. In addition, there are differences in proximity, sensitivity, density, and distribution of Ca^{2+} uptake and Ca^{2+} release units between SR and NE. All these factors may contribute to the precision sensing and release of lumenal Ca^{2+} that can produce both excitation-contraction coupling in the cytosol and excitation-transcription coupling in the nuclear regions. The experimental approaches employed in our studies, did not permit detection of downstream effects, e.g., activation of CaMKII or calcineurin, known downstream targets of IP_3 signaling pathway. Moreover, our use of permeabilized CMs may result in dialysis/loss of critical co-factors in the down-stream signal pathways. Future experiments will be required to gain greater insights into the role of PLB in regulation of the excitation-transcription coupling signal pathway.

The functional stoichiometry of PLB inhibition of SERCA2a in SR membranes has been a subject of debated [1–4]. PLB is in a dynamic equilibrium between monomers and homo-pentamers [47]. Although still controversial [48], it is likely that PLB monomers specifically interact with SERCA2a in the Ca^{2+} free, *E*2 conformation, thus preventing the pump from binding Ca^{2+} to continue the enzyme kinetic cycle [49]. Although temperature affects equilibria between PLB monomers and pentamers and PLB monomers binding to SERCA2a, PLB interacts with SERCA at room temperature [50]. In human SR membranes, there is a 1:1 molar ratio between PLB and SERCA2a [51]. In *in vitro* heterologous expression systems, increasing PLB expression beyond 1:1 over SERCA2a does not produce additional inhibition [52, 53]. On the other hand, using PLB overexpression mice, Brittsan *et*

al [54] determined that approximately 40% of SERCA2a were regulated by PLB in the SR membranes; over-expression of PLB in mice enhanced SERCA2a inhibition. In the NE, PLB maintained similar pentamer to monomer ratio to that in SR on SDS-PAGE [25]. However, in addition to the amount of PLB, regulation of SERCA may also be achieved through various signal pathways that uniquely phosphorylate PLB in the NE. Collectively, the biochemical properties of PLB in the NE remain poorly understood and need extensive further investigation.

In conclusion, as a powerful known regulator of SR Ca^{2+} uptake and release, PLB also critically regulates nuclear Ca^{2+} signaling. Regardless of the mechanism of nuclear Ca^{2+} release, our results suggest for the first time that PLB exerts effects on nuclear Ca^{2+} handling. By increasing Ca^{2+} uptake into lumen of the NE and perhaps other perinuclear membranes, the acute reversal of PLB inhibition decreases global Ca^{2+} concentration at rest in the nucleoplasm, and increases transient Ca^{2+} release into the nucleus, through mechanisms involving local IP_3R and RyR2.

Supplementary Material

Refer to Web version on PubMed Central for supplementary material.

Acknowledgments

We thank Jian Tan and Jin Guo for great technical supports. We also thank Dr. Steve Cala for the critical comments of the manuscript.

Source of Funding

This study was supported in part by American Heart Association Grant #18TPA34170284 /ZC/2018; NIH Grants TR002208–01, R01 HL139829, R01HL26057, a Medtronic-Zipes Endowment (PSC), the Indiana University Health-Indiana University School of Medicine Strategic Research Initiative; and the Dr. Charles Fisch Cardiovascular Research Award endowed by Dr. Suzanne B. Knoebel of the Krannert Institute of Cardiology; and Grant-in-Aid from the Ministry of Health, Labor and Welfare, and Health and Labor Sciences Research Grants, Japan (Research on Health Services: H27-Fund for the Promotion of Joint International Research (Fostering Joint International Research, No.15kk0330).

Abbreviations:

CM	cardiomyocyte
ER	endoplasmic reticulum
Fab	the Fab fragment of the monoclonal anti-PLB antibody 2D12
IP_3R	inositol 1,4,5-trisphosphate receptor
NE	nuclear envelope
PLB	phospholamban
RyR	ryanodine receptor
SCW	spontaneous Ca^{2+} wave
SR	sarcoplasmic reticulum

SERCA2a	isoform of Ca^{2+}-ATPase in cardiac SR
2-APB	2-aminoethoxydiphenyl borate

References

[1]. Simmerman HK, Jones LR, Phospholamban: protein structure, mechanism of action, and role in cardiac function, Physiol. Rev 78(4) (1998) 921–47. [PubMed: 9790566]

[2]. MacLennan DH, Kranias EG, Phospholamban: a crucial regulator of cardiac contractility, Nat. Rev. Mol. Cell. Biol 4(7) (2003) 566–77. [PubMed: 12838339]

[3]. Kranias EG, Hajjar RJ, Modulation of cardiac contractility by the phospholamban/SERCA2a regulatome, Circ Res 110(12) (2012) 1646–60. [PubMed: 22679139]

[4]. Kranias EG, Hajjar RJ, The Phospholamban Journey 4 Decades After Setting Out for Ithaka, Circ Res 120(5) (2017) 781–783. [PubMed: 28254803]

[5]. Luo W, Grupp IL, Harrer J, Ponniah S, Grupp G, Duffy JJ, Doetschman T, Kranias EG, Targeted ablation of the phospholamban gene is associated with markedly enhanced myocardial contractility and loss of beta-agonist stimulation, Circ Res 75(3) (1994) 401–9. [PubMed: 8062415]

[6]. Kadambi VJ, Ponniah S, Harrer JM, Hoit BD, Dorn, GW, 2nd, Walsh RA, Kranias EG, Cardiac-specific overexpression of phospholamban alters calcium kinetics and resultant cardiomyocyte mechanics in transgenic mice, J. Clin. Invest 97(2) (1996) 533–9. [PubMed: 8567978]

[7]. Schmitt JP, Kamisago M, Asahi M, Li GH, Ahmad F, Mende U, Kranias EG, MacLennan DH, Seidman JG, Seidman CE, Dilated cardiomyopathy and heart failure caused by a mutation in phospholamban, Science 299(5611) (2003) 1410–3. [PubMed: 12610310]

[8]. Haghighi K, Kolokathis F, Pater L, Lynch RA, Asahi M, Gramolini AO, Fan GC, Tsiapras D, Hahn HS, Adamopoulos S, Liggett SB, Dorn, GW, 2nd, MacLennan DH, Kremastinos DT, Kranias EG, Human phospholamban null results in lethal dilated cardiomyopathy revealing a critical difference between mouse and human, The Journal of clinical investigation 111(6) (2003) 869–76. [PubMed: 12639993]

[9]. Haghighi K, Kolokathis F, Gramolini AO, Waggoner JR, Pater L, Lynch RA, Fan GC, Tsiapras D, Parekh RR, Dorn, GW, 2nd, MacLennan DH, Kremastinos DT, Kranias EG, A mutation in the human phospholamban gene, deleting arginine 14, results in lethal, hereditary cardiomyopathy, Proc Natl Acad Sci U S A 103(5) (2006) 1388–93. [PubMed: 16432188]

[10]. Hardingham GE, Chawla S, Johnson CM, Bading H, Distinct functions of nuclear and cytoplasmic calcium in the control of gene expression, Nature 385(6613) (1997) 260–5. [PubMed: 9000075]

[11]. Stehno-Bittel L, Perez-Terzic C, Clapham DE, Diffusion across the nuclear envelope inhibited by depletion of the nuclear Ca2+ store, Science 270(5243) (1995) 1835–8. [PubMed: 8525380]

[12]. Wu X, Zhang T, Bossuyt J, Li X, McKinsey TA, Dedman JR, Olson EN, Chen J, Brown JH, Bers DM, Local InsP3-dependent perinuclear Ca2+ signaling in cardiac myocyte excitation-transcription coupling, The Journal of clinical investigation 116(3) (2006) 675–82. [PubMed: 16511602]

[13]. Zima AV, Bare DJ, Mignery GA, Blatter LA, IP3-dependent nuclear Ca2+ signalling in the mammalian heart, J Physiol 584(Pt 2) (2007) 601–11. [PubMed: 17761776]

[14]. Higazi DR, Fearnley CJ, Drawnel FM, Talasila A, Corps EM, Ritter O, McDonald F, Mikoshiba K, Bootman MD, Roderick HL, Endothelin-1-stimulated InsP3-induced Ca2+ release is a nexus for hypertrophic signaling in cardiac myocytes, Molecular cell 33(4) (2009) 472–82. [PubMed: 19250908]

[15]. Domeier TL, Zima AV, Maxwell JT, Huke S, Mignery GA, Blatter LA, IP3 receptor-dependent Ca2+ release modulates excitation-contraction coupling in rabbit ventricular myocytes, American journal of physiology. Heart and circulatory physiology 294(2) (2008) H596–604. [PubMed: 18055509]

[16]. Luo D, Yang D, Lan X, Li K, Li X, Chen J, Zhang Y, Xiao RP, Han Q, Cheng H, Nuclear Ca2+ sparks and waves mediated by inositol 1,4,5-trisphosphate receptors in neonatal rat cardiomyocytes, Cell calcium 43(2) (2008) 165–74. [PubMed: 17583790]

[17]. Escobar M, Cardenas C, Colavita K, Petrenko NB, Franzini-Armstrong C, Structural evidence for perinuclear calcium microdomains in cardiac myocytes, J Mol Cell Cardiol 50(3) (2011) 451–9. [PubMed: 21147122]

[18]. Guo A, Cala SE, Song LS, Calsequestrin accumulation in rough endoplasmic reticulum promotes perinuclear Ca2+ release, J Biol Chem 287(20) (2012) 16670–80. [PubMed: 22457350]

[19]. Kockskamper J, Zima AV, Roderick HL, Pieske B, Blatter LA, Bootman MD, Emerging roles of inositol 1,4,5-trisphosphate signaling in cardiac myocytes, J Mol Cell Cardiol 45(2) (2008) 128–47. [PubMed: 18603259]

[20]. Zima AV, Blatter LA, Inositol-1,4,5-trisphosphate-dependent Ca(2+) signalling in cat atrial excitation-contraction coupling and arrhythmias, J Physiol 555(Pt 3) (2004) 607–15. [PubMed: 14754996]

[21]. Bare DJ, Kettlun CS, Liang M, Bers DM, Mignery GA, Cardiac type 2 inositol 1,4,5-trisphosphate receptor: interaction and modulation by calcium/calmodulin-dependent protein kinase II, J Biol Chem 280(16) (2005) 15912–20. [PubMed: 15710625]

[22]. Humbert JP, Matter N, Artault JC, Koppler P, Malviya AN, Inositol 1,4,5-trisphosphate receptor is located to the inner nuclear membrane vindicating regulation of nuclear calcium signaling by inositol 1,4,5-trisphosphate. Discrete distribution of inositol phosphate receptors to inner and outer nuclear membranes, J Biol Chem 271(1) (1996) 478–85. [PubMed: 8550605]

[23]. Gerasimenko OV, Gerasimenko JV, Tepikin AV, Petersen OH, ATP-dependent accumulation and inositol trisphosphate- or cyclic ADP-ribose-mediated release of Ca2+ from the nuclear envelope, Cell 80(3) (1995) 439–44. [PubMed: 7859285]

[24]. Ljubojevic S, Radulovic S, Leitinger G, Sedej S, Sacherer M, Holzer M, Winkler C, Pritz E, Mittler T, Schmidt A, Sereinigg M, Wakula P, Zissimopoulos S, Bisping E, Post H, Marsche G, Bossuyt J, Bers DM, Kockskamper J, Pieske B, Early remodeling of perinuclear Ca2+ stores and nucleoplasmic Ca2+ signaling during the development of hypertrophy and heart failure, Circulation 130(3) (2014) 244–55. [PubMed: 24928680]

[25]. Wu AZ, Xu D, Yang N, Lin SF, Chen PS, Cala SE, Chen Z, Phospholamban is concentrated in the nuclear envelope of cardiomyocytes and involved in perinuclear/nuclear calcium handling, J Mol Cell Cardiol 100 (2016) 1–8. [PubMed: 27642167]

[26]. Chan YH, Tsai WC, Song Z, Ko CY, Qu Z, Weiss JN, Lin SF, Chen PS, Jones LR, Chen Z, Acute reversal of phospholamban inhibition facilitates the rhythmic whole-cell propagating calcium waves in isolated ventricular myocytes, J Mol Cell Cardiol 80C (2015) 126–135.

[27]. Harzheim D, Movassagh M, Foo RS, Ritter O, Tashfeen A, Conway SJ, Bootman MD, Roderick HL, Increased InsP3Rs in the junctional sarcoplasmic reticulum augment Ca2+ transients and arrhythmias associated with cardiac hypertrophy, Proc Natl Acad Sci U S A 106(27) (2009) 11406–11. [PubMed: 19549843]

[28]. Sleiman NH, McFarland TP, Jones LR, Cala SE, Transitions of protein traffic from cardiac ER to junctional SR, J Mol Cell Cardiol 81C (2015) 34–45.

[29]. Li Y, Kranias EG, Mignery GA, Bers DM, Protein kinase A phosphorylation of the ryanodine receptor does not affect calcium sparks in mouse ventricular myocytes, Circ Res 90(3) (2002) 309–16. [PubMed: 11861420]

[30]. Yang Z, Steele DS, Characteristics of prolonged Ca2+ release events associated with the nuclei in adult cardiac myocytes, Circ Res 96(1) (2005) 82–90. [PubMed: 15569829]

[31]. Soeller C, Jacobs MD, Jones KT, Ellis-Davies GC, Donaldson PJ, Cannell MB, Application of two-photon flash photolysis to reveal intercellular communication and intracellular Ca2+ movements, J Biomed Opt 8(3) (2003) 418–27. [PubMed: 12880347]

[32]. Huser J, Bers DM, Blatter LA, Subcellular properties of [Ca2+]i transients in phospholamban-deficient mouse ventricular cells, The American journal of physiology 274(5 Pt 2) (1998) H1800–11. [PubMed: 9612393]

[33]. Wu X, Bers DM, Sarcoplasmic reticulum and nuclear envelope are one highly interconnected Ca2+ store throughout cardiac myocyte, Circ Res 99(3) (2006) 283–91. [PubMed: 16794184]

[34]. Kockskamper J, Seidlmayer L, Walther S, Hellenkamp K, Maier LS, Pieske B, Endothelin-1 enhances nuclear Ca2+ transients in atrial myocytes through Ins(1,4,5)P3-dependent Ca2+ release from perinuclear Ca2+ stores, Journal of cell science 121(Pt 2) (2008) 186–95. [PubMed: 18089647]

[35]. Jiang D, Xiao B, Yang D, Wang R, Choi P, Zhang L, Cheng H, Chen SR, RyR2 mutations linked to ventricular tachycardia and sudden death reduce the threshold for store-overload-induced Ca2+ release (SOICR), Proc Natl Acad Sci U S A 101(35) (2004) 13062–7. [PubMed: 15322274]

[36]. Plackic J, Preissl S, Nikonova Y, Pluteanu F, Hein L, Kockskamper J, Enhanced nucleoplasmic Ca(2+) signaling in ventricular myocytes from young hypertensive rats, J Mol Cell Cardiol 101 (2016) 58–68. [PubMed: 27816525]

[37]. Liu GS, Morales A, Vafiadaki E, Lam CK, Cai WF, Haghighi K, Adly G, Hershberger RE, Kranias EG, A novel human R25C-phospholamban mutation is associated with super-inhibition of calcium cycling and ventricular arrhythmia, Cardiovasc Res 107(1) (2015) 164–74. [PubMed: 25852082]

[38]. Karakikes I, Stillitano F, Nonnenmacher M, Tzimas C, Sanoudou D, Termglinchan V, Kong CW, Rushing S, Hansen J, Ceholski D, Kolokathis F, Kremastinos D, Katoulis A, Ren L, Cohen N, Gho JM, Tsiapras D, Vink A, Wu JC, Asselbergs FW, Li RA, Hulot JS, Kranias EG, Hajjar RJ, Correction of human phospholamban R14del mutation associated with cardiomyopathy using targeted nucleases and combination therapy, Nature communications 6 (2015) 6955.

[39]. Haghighi K, Pritchard T, Bossuyt J, Waggoner JR, Yuan Q, Fan GC, Osinska H, Anjak A, Rubinstein J, Robbins J, Bers DM, Kranias EG, The human phospholamban Arg14-deletion mutant localizes to plasma membrane and interacts with the Na/K-ATPase, J Mol Cell Cardiol 52(3) (2012) 773–82. [PubMed: 22155237]

[40]. Bai Y, Jones PP, Guo J, Zhong X, Clark RB, Zhou Q, Wang R, Vallmitjana A, Benitez R, Hove-Madsen L, Semeniuk L, Guo A, Song LS, Duff HJ, Chen SR, Phospholamban knockout breaks arrhythmogenic Ca(2)(+) waves and suppresses catecholaminergic polymorphic ventricular tachycardia in mice, Circ Res 113(5) (2013) 517–26. [PubMed: 23856523]

[41]. Keller M, Kao JP, Egger M, Niggli E, Calcium waves driven by “sensitization” wave-fronts, Cardiovasc Res 74(1) (2007) 39–45. [PubMed: 17336953]

[42]. Chu G, Luo W, Slack JP, Tilgmann C, Sweet WE, Spindler M, Saupe KW, Boivin GP, Moravec CS, Matlib MA, Grupp IL, Ingwall JS, Kranias EG, Compensatory mechanisms associated with the hyperdynamic function of phospholamban-deficient mouse hearts, Circ Res 79(6) (1996) 1064–76. [PubMed: 8943945]

[43]. Chu G, Kerr JP, Mitton B, Egnaczyk GF, Vazquez JA, Shen M, Kilby GW, Stevenson TI, Maggio JE, Vockley J, Rapundalo ST, Kranias EG, Proteomic analysis of hyperdynamic mouse hearts with enhanced sarcoplasmic reticulum calcium cycling, FASEB journal : official publication of the Federation of American Societies for Experimental Biology 18(14) (2004) 1725–7. [PubMed: 15358683]

[44]. Ljubojevic S, Walther S, Asgarzoei M, Sedej S, Pieske B, Kockskamper J, In situ calibration of nucleoplasmic versus cytoplasmic Ca(2)+ concentration in adult cardiomyocytes, Biophys J 100(10) (2011) 2356–66. [PubMed: 21575569]

[45]. Lipp P, Thomas D, Berridge MJ, Bootman MD, Nuclear calcium signalling by individual cytoplasmic calcium puffs, EMBO J 16(23) (1997) 7166–73. [PubMed: 9384593]

[46]. Foskett JK, White C, Cheung KH, Mak DO, Inositol trisphosphate receptor Ca2+ release channels, Physiological reviews 87(2) (2007) 593–658. [PubMed: 17429043]

[47]. Simmerman HK, Kobayashi YM, Autry JM, Jones LR, A leucine zipper stabilizes the pentameric membrane domain of phospholamban and forms a coiled-coil pore structure, J. Biol. Chem 271(10) (1996) 5941–6. [PubMed: 8621468]

[48]. James ZM, McCaffrey JE, Torgersen KD, Karim CB, Thomas DD, Protein-protein interactions in calcium transport regulation probed by saturation transfer electron paramagnetic resonance, Biophys J 103(6) (2012) 1370–8. [PubMed: 22995510]

[49]. Akin BL, Hurley TD, Chen Z, Jones LR, The structural basis for phospholamban inhibition of the calcium pump in sarcoplasmic reticulum, J Biol Chem 288(42) (2013) 30181–91. [PubMed: 23996003]

[50]. Chen Z, Stokes DL, Rice WJ, Jones LR, Spatial and Dynamic Interactions between Phospholamban and the Canine Cardiac Ca2+ Pump Revealed with Use of Heterobifunctional Cross-linking Agents, J. Biol. Chem 278(48) (2003) 48348–56. [PubMed: 12972413]

[51]. Akin BL, Jones LR, Characterizing phospholamban to sarco(endo)plasmic reticulum Ca2+-ATPase 2a (SERCA2a) protein binding interactions in human cardiac sarcoplasmic reticulum vesicles using chemical cross-linking, J Biol Chem 287(10) (2012) 7582–93. [PubMed: 22247554]

[52]. Chen Z, Competitive displacement of wild-type phospholamban from the Ca-free cardiac calcium pump by phospholamban mutants with different binding affinities, J Mol Cell Cardiol 76c (2014) 130–137.

[53]. Chen Z, A phospholamban-tethered cardiac Ca2+ pump reveals stoichiometry and dynamic interactions between the two proteins, Biochem J 439(2) (2011) 313–9. [PubMed: 21728996]

[54]. Brittsan AG, Carr AN, Schmidt AG, Kranias EG, Maximal inhibition of SERCA2 Ca(2+) affinity by phospholamban in transgenic hearts overexpressing a non-phosphorylatable form of phospholamban, J Biol Chem 275(16) (2000) 12129–35. [PubMed: 10766848]

[55]. Picht E, Zima AV, Blatter LA, Bers DM, SparkMaster: automated calcium spark analysis with ImageJ, American journal of physiology. Cell physiology 293(3) (2007) C1073–81. [PubMed: 17376815]

Highlights:

- Phospholamban (PLB) is concentrated in nuclear envelope (NE) of cardiomyocytes (CMs).
- The Fab fragment of PLB antibody increased the lumenal Ca inside the NE of CM nuclei.
- Anti-PLB Fab increased Ca release in the nuclear regions of permeabilized CMs.
- Anti-PLB Fab decreased Ca levels elevated by IP_3 at rest in the nuclear regions.
- PLB regulates nuclear Ca handling in CMs through mechanisms involving IP_3R and RyR.

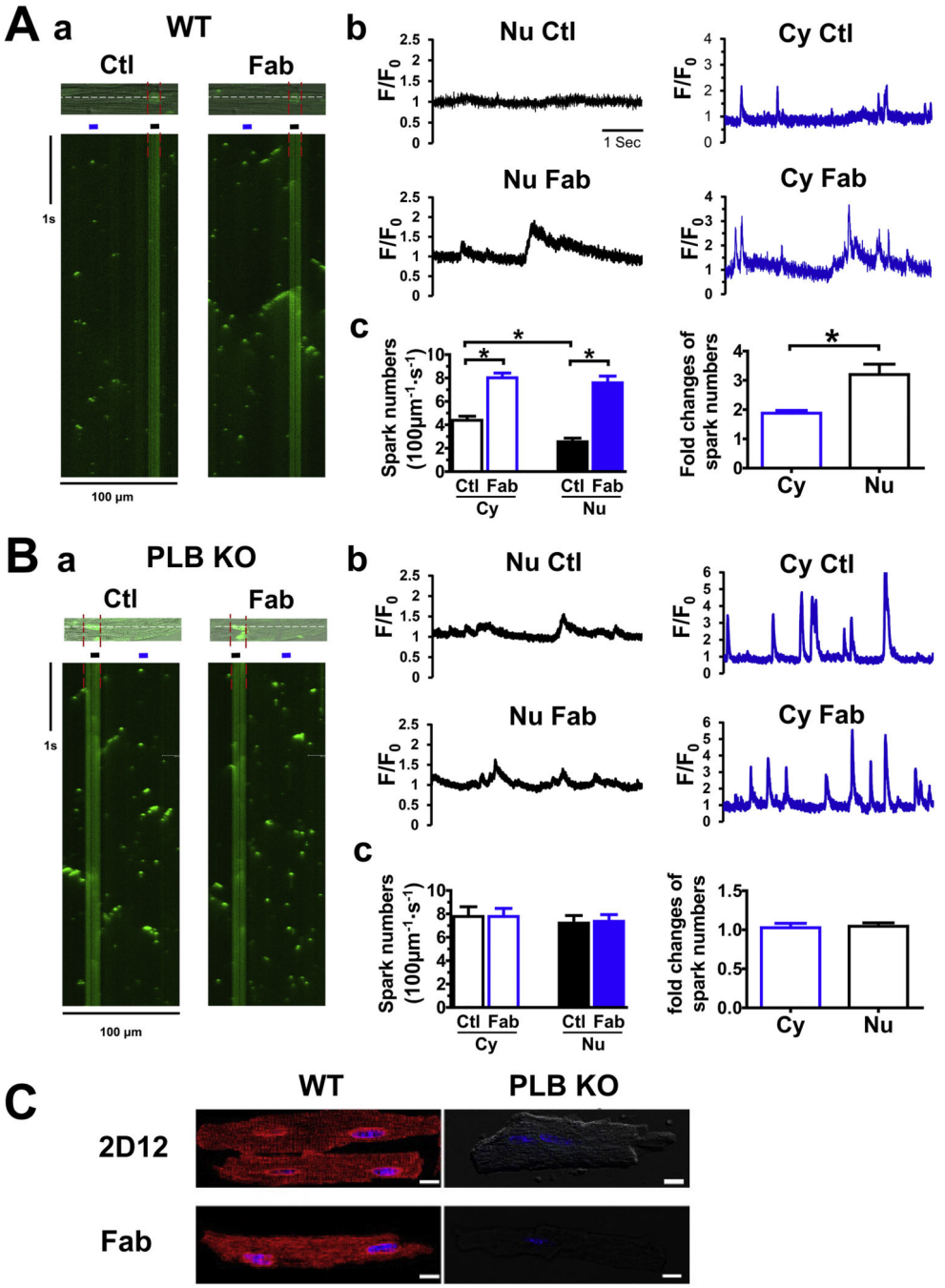

Figure 1. The effect of anti-PLB Fab on intracellular Ca^{2+} release in nuclear and cytoplasmic regions of CMs isolated from WT (A) or PLB-KO mice (B).

a. representative confocal line-scan Ca^{2+} images using Fluo-4 Ca^{2+} indicator were obtained in the same permeabilized mouse CM (*top*) before (*Ctl*) and after addition of 100 μg/ml anti-PLB Fab (*Fab*). Nucleus is between *red lines*. Scan-line (*white*) is across cytosol and nucleus. Ca^{2+} concentration was 50 nM. b. Traces showed intensity of fluorescent signals (F/F_0) across the cytosol and nucleus (regions indicated by lines in *a*). c. Bar graphs showing spark frequency in the cytoplasmic and perinuclear regions, and fold of increase after addition of anti-PLB Fab. * indicates $p<0.05$ vs control (average of 12 CMs from 5 mice). C.

Confocal immunofluorescence images showing 2D12 and anti-PLB Fab conjugated with Alexa Fluor-594 staining CMs from WT, but not from PLB-KO mice. Similar staining was obtained from at least 6 CMs isolated from WT or PLB-KO mice.

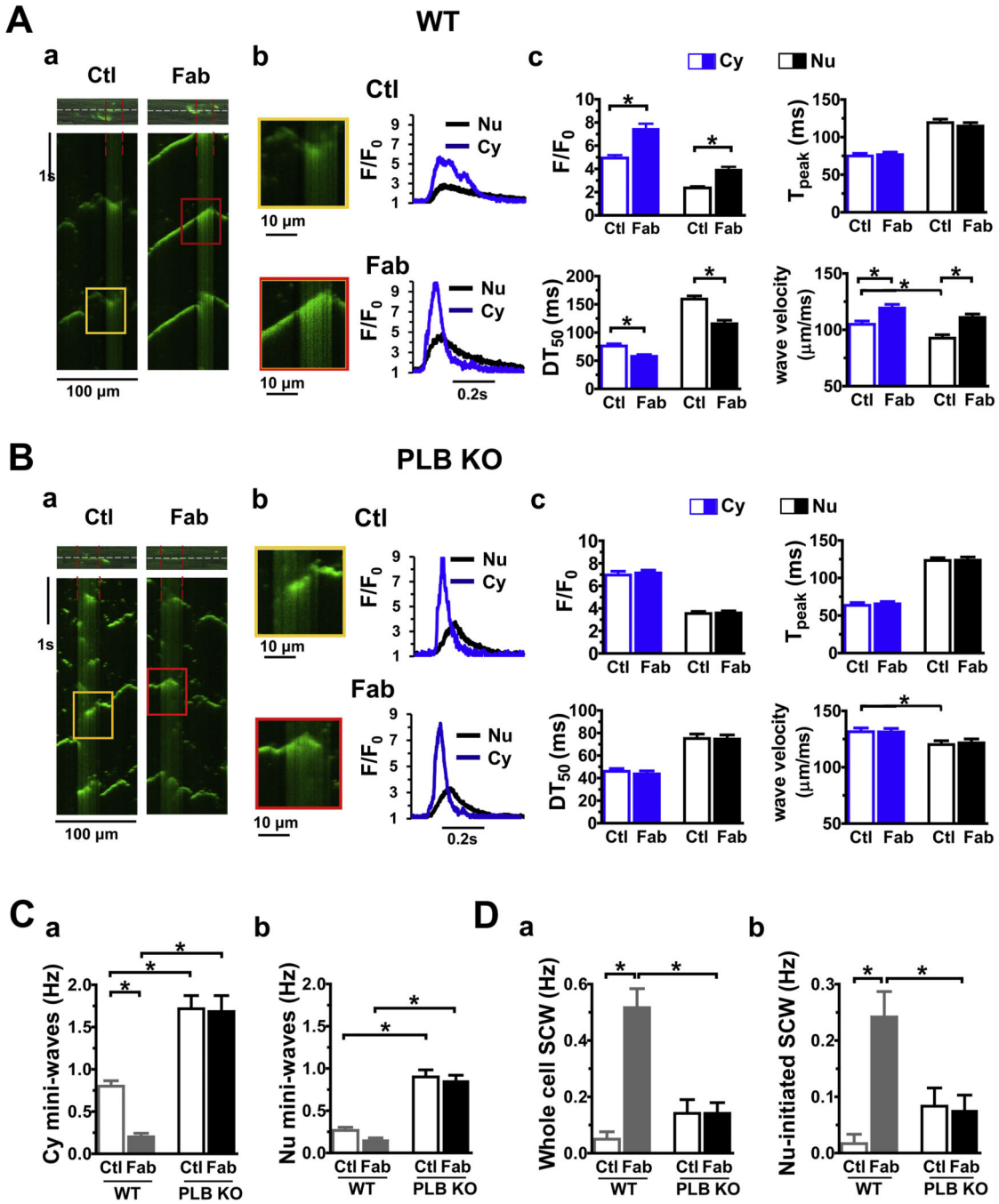

Figure 2. The effect of anti-PLB Fab on initiation of the spontaneous Ca^{2+} waves in cytoplasmic and perinuclear regions of CMs from WT (A) or PLB-KO mice (B).

a. representative confocal line-scan Ca^{2+} images using Fluo-4 Ca^{2+} indicator were obtained in the same permeabilized mouse CM (*top*) before (*Ctl*) and after addition of 100 μg/ml anti-PLB Fab (*Fab*). Nucleus is between *red lines*. Scan-line (*white*) is over cytosol and nucleus. Ca^{2+} concentration was 100 nM. b. Magnified region showing spontaneous Ca^{2+} waves (SCWs). Traces showed intensity of fluorescent signals (F/F_0) of SCWs. c. Bar graphs showing characteristics of SCWs. C, D. Bar graphs showing frequency of mini-waves and

long SCWs initiated at cytoplasmic and perinuclear regions. * indicates $p<0.05$ vs control (average of 12 CMs from 5 WT or 12 CMs from 5 PLB KO mice, respectively).

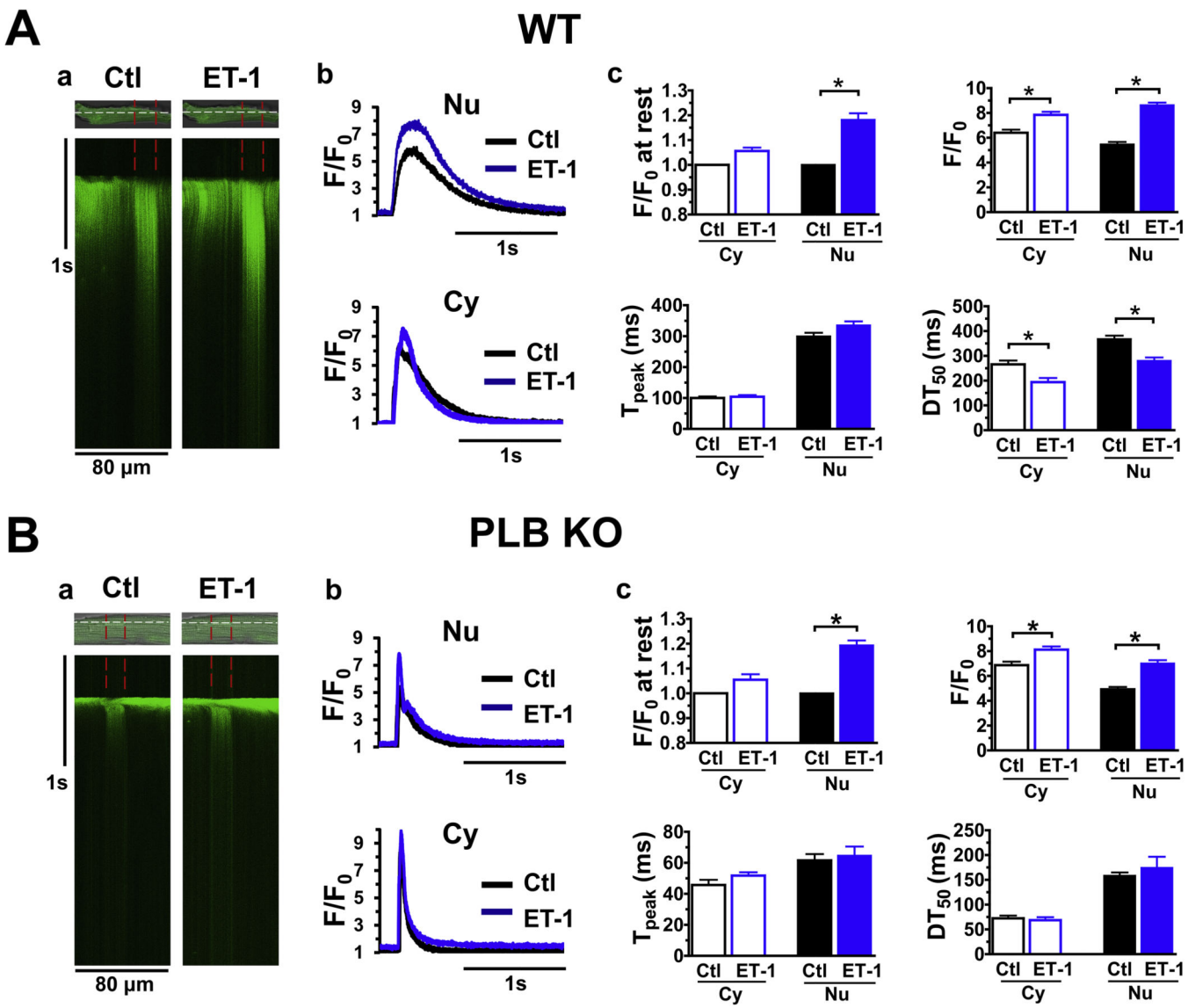

Figure 3. The effect of ET-1 (100 nM) on Ca^{2+} transients in cytoplasmic and perinuclear regions of CMs isolated from WT (A) or PLB-KO mice (B).

a. representative traces of Ca^{2+} transients in cytoplasmic and perinuclear (between red lines) regions of CMs. b and c, intensity profiles and biophysical parameters of Ca^{2+} transients in cytoplasmic and perinuclear regions of CMs. Each Ca transient have its own diastolic Ca level diastolic Ca in the absence of ET was used for F0 determination. * indicates $p<0.05$ vs control (average of 10 CMs from 5 WT or 10 CMs from 5 PLB KO mice, respectively).

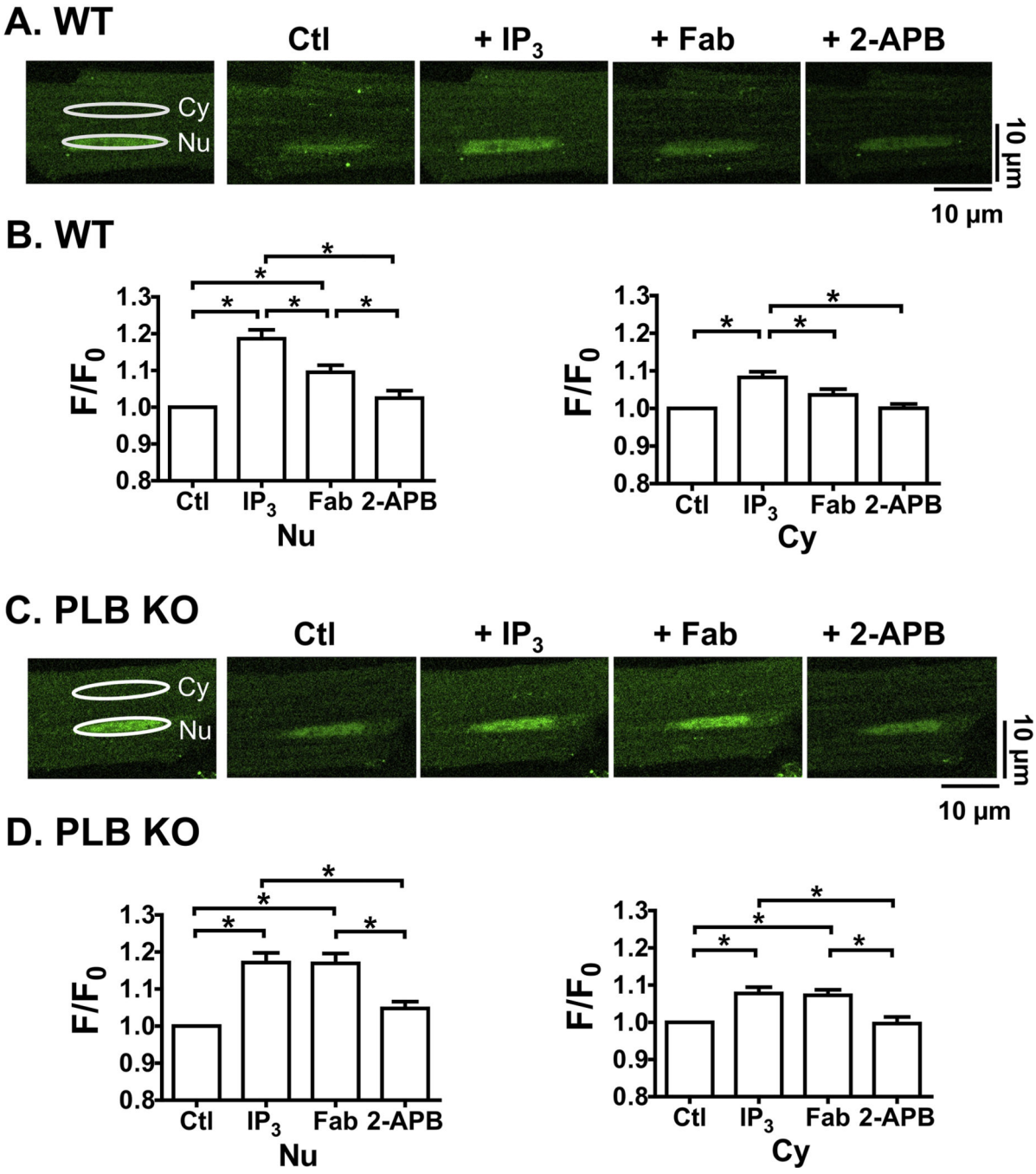

Figure 4. Anti-PLB Fab affects IP_3-induced nuclear Ca^{2+} releases at rest in WT (A, B) but not in PLB-KO (C, D).

Representative 2D confocal images show fluo-4 signals in permeabilized CMs. $[Ca^{2+}]_I$ = 10 nM. A.C, Scan Images for nuclear (Nu) and cytosolic (Cy) regions show fluo-4 signals and intensity (*F/F0*) at control condition (Ctl) and 3 min after sequential addition of IP_3 (10 μM), anti-PLB Fab (100μg/ml) and IP_3R blocker 2-APB (10 μM). White ellipses show the identical regions of interest for detecting fluorescence intensity in Nu and Cy. B.D, plots show *F/F0* at rest for Nu (*left panels*) and Cy (*right panels*) in each condition. * indicates $p<0.05$. n=12 CMs, 6 mice for WT; n= 12 CMs, 6 mice for PLB-KO.

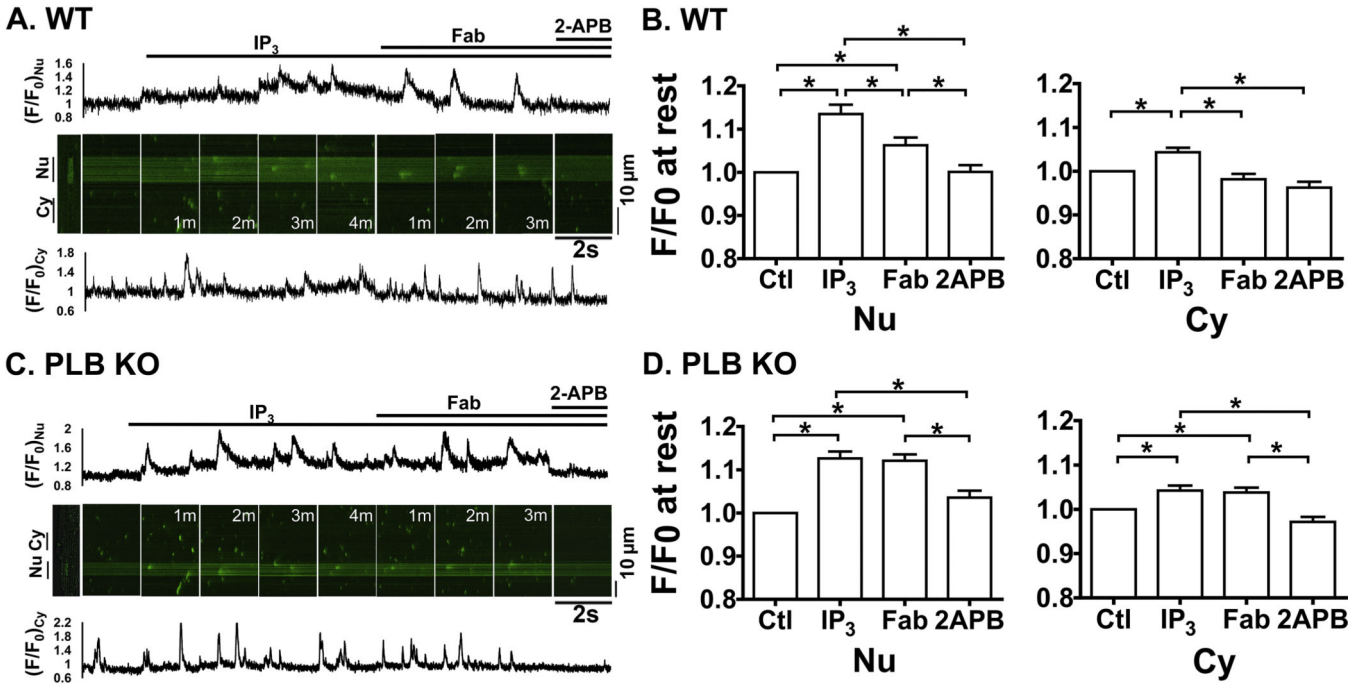

Figure 5. Anti-PLB Fab affects IP_3-induced nuclear Ca^{2+} releases at 50nM $[Ca^{2+}]_i$ in WT (A,B) but not in PLB-KO (C,D).

Representative line-scan confocal images show fluo-4 signals in permeabilized CMs. $[Ca^{2+}]_i$,=50 nM. A, C. Scan Images (2 sec) and traces for nuclear (Nu, *upper panels*) and cytosolic (Cy, *lower panels*) regions show fluo-4 signals and intensity profiles (F/F_0) at basal condition (Ctl) and after sequential addition of IP_3 (10 μM), anti-PLB Fab (100μg/ml), and 2-APB (10 μM). M indicates minutes after addition of the reagents. B.D, Bar graphs show F/F_0 at rest for Nu (*left panels*) and Cy (*right panels*) in each condition. * indicates $p<0.05$. n=12 CMs, 6 mice for WT; n= 13 CMs, 6 mice for PLB-KO.

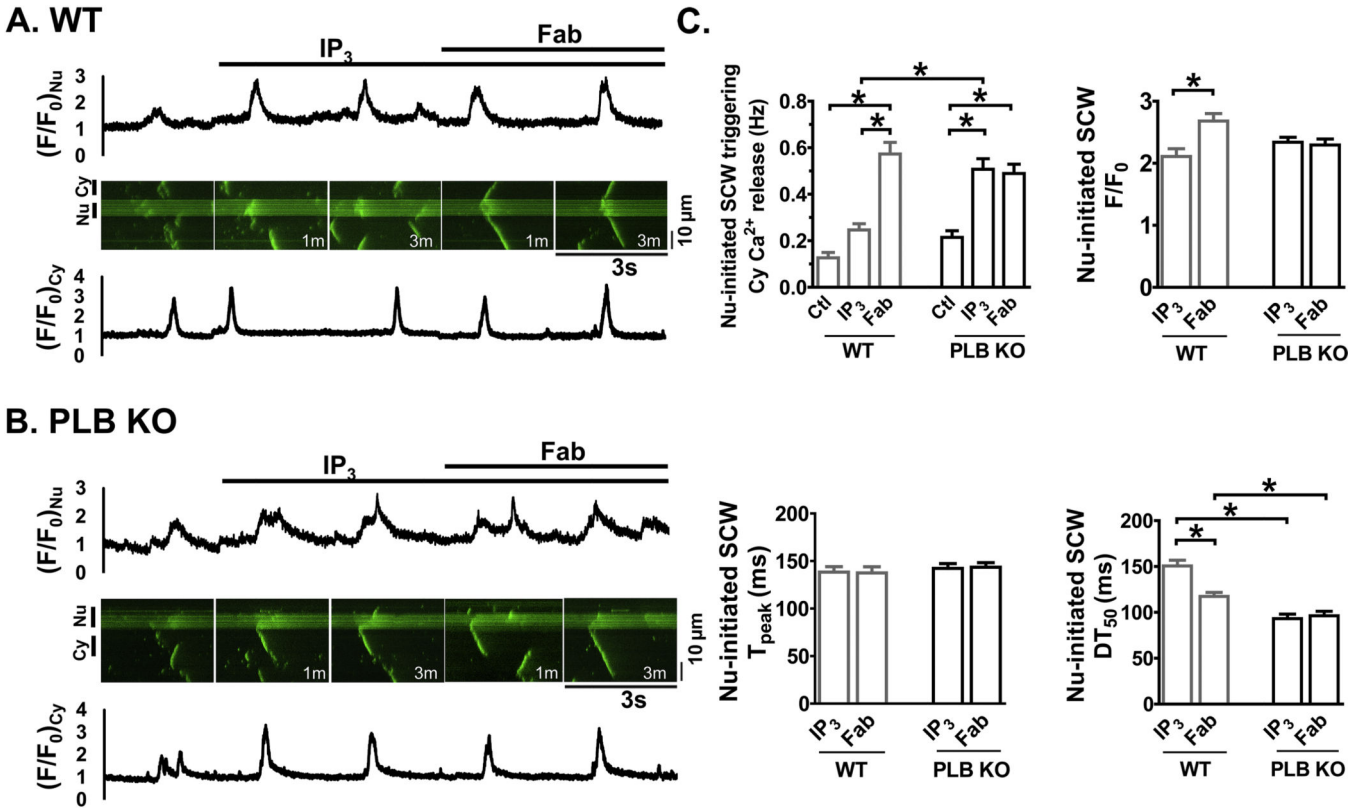

Figure 6. Anti-PLB Fab affects IP_3-induced SCWs originated from nuclear regions in WT (A) but not in PLB-KO (B).

Representative line-scan confocal images show fluo-4 signals in permeabilized CMs. </P/> $[Ca^{2+}]_i$,=100nM. A, B. Scan images (3 sec) and traces for cytosolic (Cy, *lower panels*) and nuclear (Nu, *upper panels*) regions show fluo-4 signals and intensity profiles (F/F_0) at basal (Ctl) and after sequential addition of IP_3 (10 μM) and anti-PLB Fab (100μg/ml). M indicates minutes after addition of the reagents. C. Plot shows the frequency and kinetic parameters of nuclear initiated SCWs with triggering cytosolic Ca^{2+} release. * indicates $p<0.05$. n=15 CMs, 7 mice for WT; n= 14 CMs, 7 mice for PLB-KO.

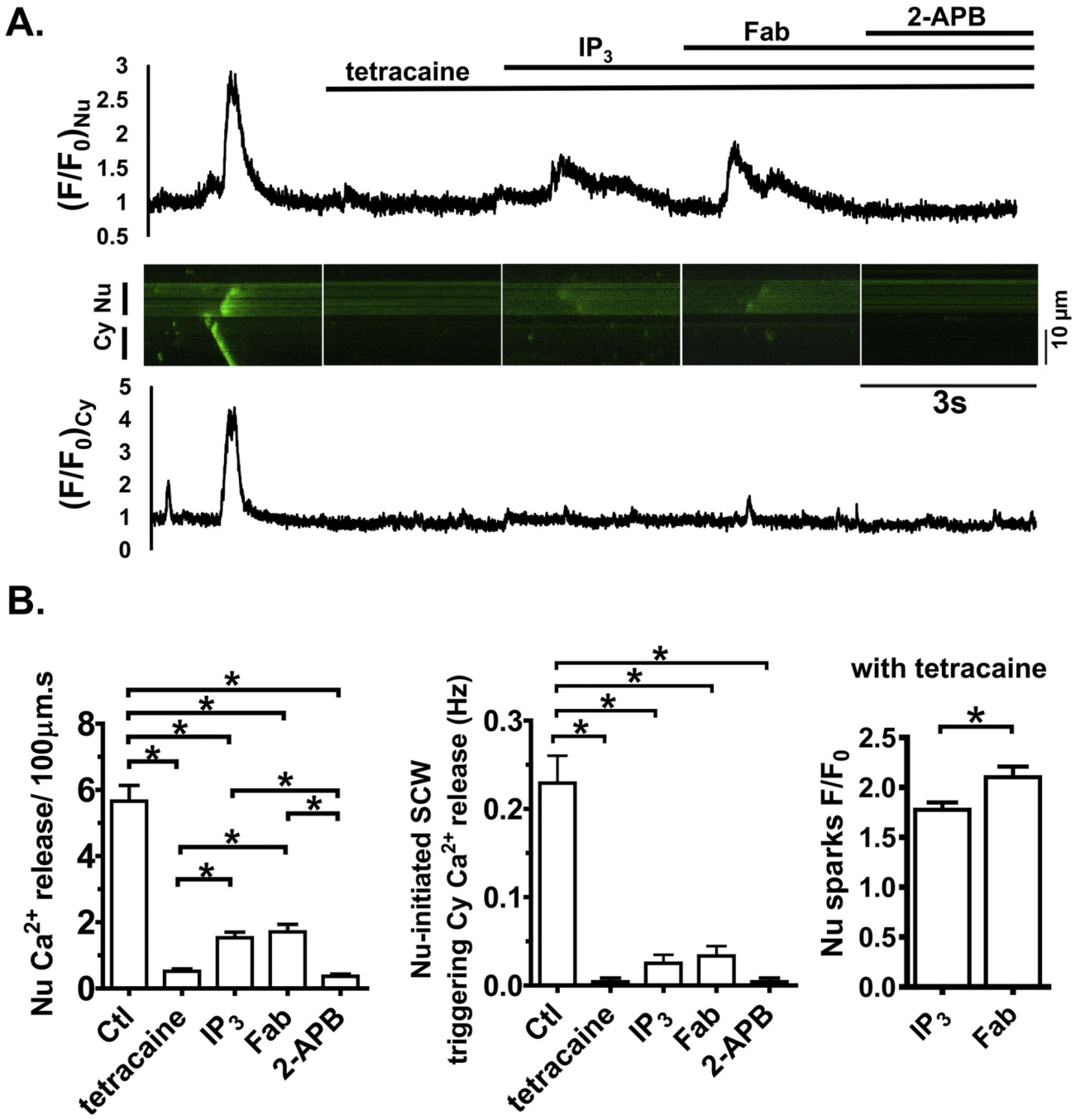

Fig. 7. Effects of anti-PLB Fab with pretreatment of tetracaine and IP_3 in WT.

A. Representative line-scan confocal images and intensity profiles (F/F_0) of fluo-4 signals in cytoplasmic and nuclear regions at baseline and 3 minutes after sequential addition of tetracaine (0.5 mM), IP_3 (10 μM), anti-PLB Fab (100 μg/ml), and 2-APB (10 μM). B. Bar graphs show characteristics of Ca^{2+} release. n= 12 CMs from 6 WT mice.

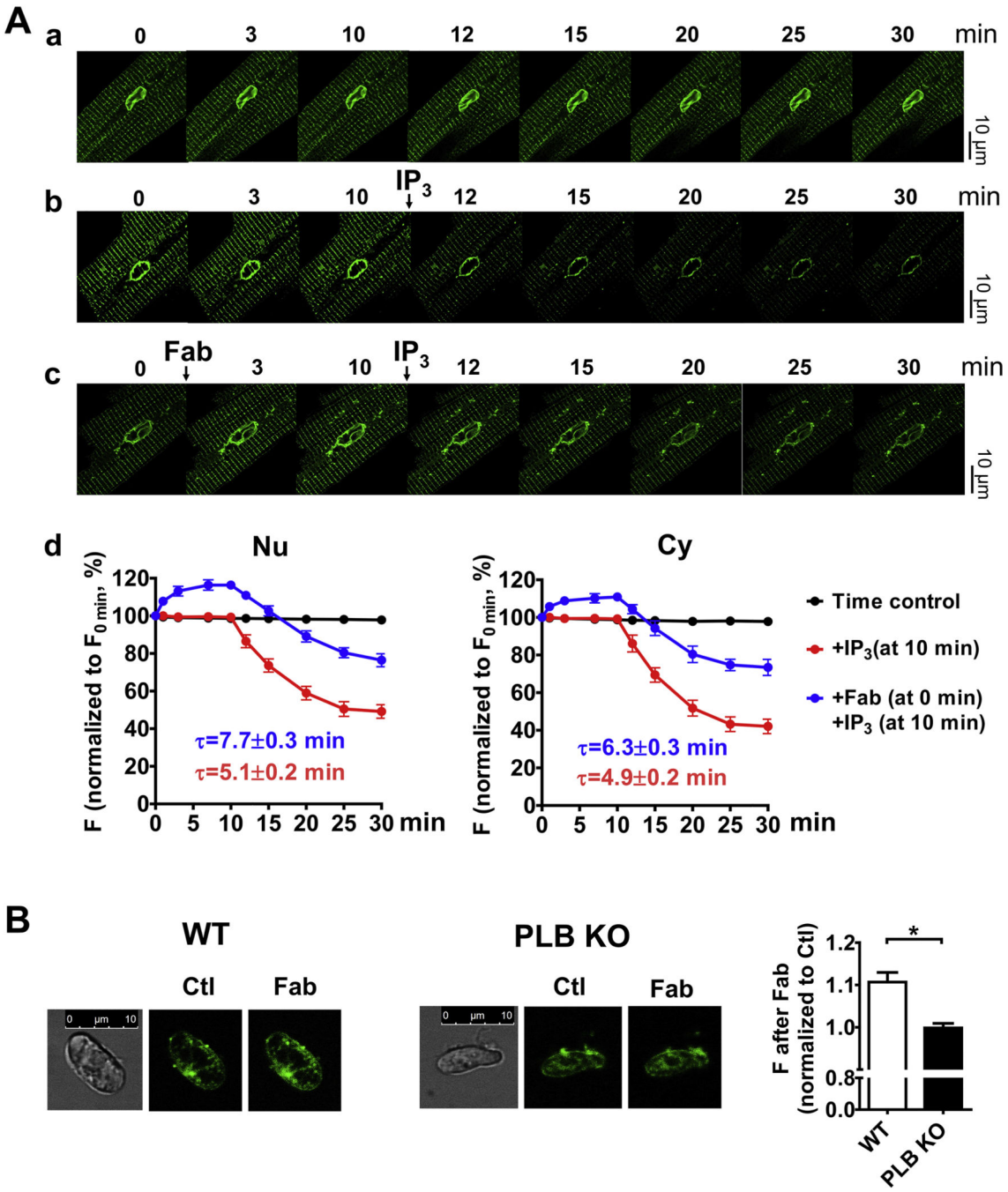

Fig. 8. Effects of anti-PLB Fab on Ca^{2+} concentration in the lumen of NE and SR.

Permeabilized CMs or isolated cardiac nuclei from both WT and PLB-KO mice were loaded with mag-fluo-4 and imaged. A. Representative 2D confocal images of mag-fluo-4 signals in the NE and SR from permeabilized dog CMs at a. baseline; b. after addition of IP_3 (10 μM); and c. sequential addition of anti-PLB Fab (100 μg/ml), and IP_3 (10 μM). d. graphs show time-dependent intensity profiles (F/F_{0min}) after treatments. n= 6 CMs from 2 dogs. B. Representative 2D confocal images of mag-fluo-4 signals in the NE in isolated cardiac

nuclei from WT and PLB-KO mice at control (Ctl) and after addition of anti-PLB Fab (Fab). Bar graph shows the mag-fluo-4 intensity ratios after addition of anti-PLB Fab.

Table 1.

Characteristics of Ca^{2+} sparks.

Ca^{2+} activities were measured at 50 nM of $[Ca^{2+}]_i$ in permeabilized CMs from WT and PLB-KO as indicated in Fig. 5. Ca^{2+} sparks were measured at baseline, after IP_3, after anti-PLB Fab and 2-APB and analyzed using the SparkMaster plug-in for ImageJ software [55]. Parameters of Ca^{2+} sparks characteristics were compared 6 using one-way ANOVA with Tukey post-tests. Results are the means ± SEM from 12 CMs from 6 WT and 13 7 CMs from 6 PLB KO mice. * indicates P<0.05 vs baseline, † vs. IP3, ‡ vs. Fab. FWHM: full width at half 8 maximum; FDHM: full duration half maximum; DT_{50}: half decay time.

WT Nu	**Spark numbers (/100 μm.s)**	**Peak amplitude F/F_0**	**FWHM, μm**	**FDHM, ms**	**DT_{50}, ms**
control	2.6 ± 0.5	1.8 ± 0.1	1.7 ± 0.2	30.4 ± 3.9	36.5 ± 6.0
IP_3	8.3 ± 0.9 *	1.8 ± 0.1	1.9 ± 0.1	35.0 ± 3.6	52.6 ± 11.6
Fab	8.8 ± 0.8 *	2.2 ± 0.1 *†	2.8 ± 0.2 *†	69.1 ± 6.6 *†	118.6 ± 29.9 *†
2-APB	2.3 ± 0.4 †‡	1.8 ± 0.1 ‡	1.7 ± 0.2 ‡	28.0 ± 4.4 ‡	29.7 ± 3.2 ‡
WT Cy					
control	4.3 ± 0.4	3.1 ± 0.1	2.9 ± 0.1	28.9 ± 1.4	24.2 ± 1.4
IP_3	6.4 ± 0.8	3.3 ± 0.1	3.0 ± 0.1	27.9 ± 0.8	28.2 ± 1.7
Fab	8.3 ± 0.5 *	4.2 ± 0.1 *†	3.8 ± 0.1 *†	40.2 ± 1.9 *†	37.2 ± 1.9 *†
2-APB	3.9 ± 0.6 †‡	2.9 ± 0.1 ‡	2.8 ± 0.1 ‡	26.1 ± 1.0 ‡	29.9 ± 1.9 ‡
KO Nu					
control	5.6 ± 0.4	1.9 ± 0.1	1.7 ± 0.2	32.0 ± 3.8	38.5 ± 5.7
IP_3	8.6 ± 0.4 *	2.3 ± 0.1 *	2.8 ± 0.2 *	67.5 ± 4.2 *	107.8 ± 7.6 *
Fab	8.4 ± 0.3 *	2.3 ± 0.1 *	2.8 ± 0.2 *	65.3 ± 4.0 *	103.6 ± 7.3 *
2-APB	4.2 ± 0.3 †‡	1.9 ± 0.1 †‡	1.9 ± 0.2 †‡	40.9 ± 5.7 †‡	58.8 ± 14.3 †‡
KO Cy					
control	7.5 ± 0.6	3.3 ± 0.1	2.9 ± 0.1	28.6 ± 1.0	27.0 ± 1.2
IP_3	9.7 ± 0.7	3.8 ± 0.1 *	3.1 ± 0.1	32.4 ± 1.7	30.7 ± 2.0
Fab	9.5 ± 0.6	3.8 ± 0.1 *	3.1 ± 0.1	31.8 ± 1.5	31.0 ± 2.2
2-APB	5.4 ± 0.5 †‡	3.3 ± 0.1 †‡	2.7 ± 0.1	27.5 ± 1.3	29.6 ± 1.6